Optical Scanning Holography for 3-D Imaging of Fluorescent Objects in Turbid Media

by

Taegeun Kim

Thesis submitted to the Faculty of the
Virginia Polytechnic Institute and State University
in partial fulfillment of the requirements for the degree of

Master of Science
in
Electrical Engineering

Dr. Ting-Chung Poon, Chair
Dr. Guy J. Indebetouw
Dr. Hugh F. VanLandingham

December 9, 1997
Blacksburg, Virginia

Keywords: Holography, 3-D imaging, Fluorescence,Turbid media

Optical Scanning Holography for 3-D Imaging of Fluorescent Objects in Turbid Media

by

Taegeun Kim

Ting-Chung Poon, Chairman

Electrical Engineering Department

(ABSTRACT)

A holographic recording method using an optical heterodyne 2-D scanning technique for 3-D imaging of fluorescent objects in turbid media is described and experimentally demonstrated. For the first time, 3-D imaging of fluorescent objects in turbid media by a holographic method is achieved, and the diffused photon rejecting process through a heterodyne technique is analyzed. We also propose and realize a multiplexing and a digital decoding method for removing twin-image noise in optical scanning holography. The holographic method studied can be applied to 3-D biomedical imaging of fluorescent objects in turbid media as well as diffusely reflecting objects.

Acknowledgments

I wish to express my sincere thanks to my advisor, Professor Ting-Chung Poon for his guidance, support and encouragement throughout my program of study and Professor Guy J. Indebetouw who gave me a great opportunity to work with him. It has been a pleasure working with them. I am greatly indebted to Professors Poon and Indebetouw for their support and understanding which helped me through a difficult period.

I wish to thank Professor Hugh F. VanLandingham for serving on my committee and for useful suggestions and comments.

Many people have helped me throughout my program of study. I wish to thank Jae Hong Park, Jong Hyung Lee and Kyung Kyun Bae for their several useful discussions.

Finally, I wish to thank to my parents (Pyung Kwang Kim, Ae Sook Kim), sister (Jae Hee Kim) and grandmother (Soon Lim Cho) for their endless support and encouragement.

Table of Contents

List of Figures

Chapter 1 Introduction

One of the most challenging problems in imaging is to see an object hidden in or behind a turbid medium. Many different approaches have been introduced to solve this problem, and these approaches can be divided into two large categories [1,2,3]. In one class of approaches, one attempts to image the object by detecting ballistic photons (coherent wave) selectively against a usually large background of multiply scattered photons (diffused wave). In the other class of approaches, one attempts to recover the image by the use of theoretical models of photon migration in turbid media. Since ballistic photons are unscattered or are scattered only a few-times, these photons retain some correlation with the source and, therefore, it is believed that the ballistic component of the wave is the least distorted and can be used to form an image through the turbid media [4]. The selective detection of ballistic photons can be performed by using the unique properties of the ballistic photons against the multiply scattered photons, as ballistic photons (coherent wave) arrive earlier than the diffused photons (diffused wave) and have directional, spatial, temporal and polarization coherence. Selective detection techniques include the time gating method (by the use of the first arriving property of ballistic photons), confocal imaging (by the use of directional coherence of ballistic photons), the holographic and interferometric gating method (by the use of spatial coherence of ballistic photons), the heterodyne method (by the use of the temporal coherence of ballistic photons), and the polarization method for selecting ballistic photons that have polarization coherence.

The 3-D imaging of fluorescent objects in turbid media is a particularly interesting problem for noninvasive medical probing [5,6]. Some ballistic photon detection methods have been applied to this problem. The other approach, using a theoretical model of photon migration for imaging in turbid media, is aimed to create the image of an object

with diffused photons [5,7]. Even though the image from the diffused wave is very distorted because of multiple scattering, we can reconstruct the object's image if we can analyze how the wave has been distorted. With this approach, we can image the object through dense media where virtually no ballistic photons survive. However this method involves intensive inverse problems and the results are highly dependent on the model or algorithm.

In this thesis, we apply a heterodyne optical scanning holographic method [8,9] to 3-D imaging of fluorescent objects in turbid media. We extract the ballistic photons by the use of the spatial and temporal coherence property of these ballistic photons. This is obtained by simultaneous use of holographic and heterodyne selective detection. Although the fluorescent light does not have coherence with the illuminating light, we can still use the coherent selective detection technique and create a hologram. This can be done because the optical scanning holographic recording is performed by a spatially encoded coherent scanning beam (Fresnel zone pattern), and the holographic information is encoded by the interaction between this coherent scanning beam and the spatial distribution of a fluorescent object. This is one of the unique properties of optical scanning holography (OSH) [11]. In addition, we extract the ballistic photons through the heterodyne process inherent in optical scanning holography. In Chapter 3, the optical scanning holographic process for imaging fluorescent objects in a turbid medium is described and the diffused photon rejecting process is analyzed.

One of the most undesirable types of noise in holography is twin-image noise [14]. In Chapter 4, we review the electronic multiplexing method and the digital decoding method [10,15] for eliminating twin image noise in optical scanning holography. These methods are then applied to fluorescent optical scanning holography. In order to overcome the Nyquist limitation of the digital decoding method, we propose an adjusted digital filter for twin-image elimination and demonstrate its advantages over existing algorithms.

2. Optical properties of fluorescence

The image formation properties of a fluorescent object is different from those of an opaque or scattering object. This difference comes from the nature of the generation mechanism of fluorescent light [12]. In this section, we will review the fluorescence process and the optical properties of fluorescent light. Information in this chapter derives from chapter 7 of Optical Methods in Biology by Elizabeth M. Slayter [12]

2.1 Fluorescence

When light energy incidents on matter is absorbed, it can be transformed to heat, or can initiate a photo chemical reaction and be reradiated as fluorescence or phosphorescence. We can describe the fluorescence as the "immediate" re-emission of absorbed light energy, with some loss of energy in the form of heat or in the initiating photo chemical reactions. Even though the absorption bandwidth and fluorescence bandwidth of a molecule overlap, the fluorescence wavelengths extend to longer values than those absorbed.

From the quantum mechanical viewpoint, fluorescence is defined as "allowed" energy level transitions with the photo emission of absorbed light energy. After absorption, there is a quantum loss of vibration energy, because the excited life time is long enough for the molecule to undergo many cycles of vibration. Thus, during the excited life time, the molecule loses its energy through many cycles of vibration. This is called "Vibrational relaxation". After losing energy during a excited lifetime that is of the order of $10^{-8} sec$, the molecule decays to the ground state by fluorescence emission. After this vibrational energy loss, the molecule has reached the lowest vibrational level of the excited state which is the smallest energy level above the ground state. The maximum fluorescence intensity occurs at a wave length corresponding to the decay from the most probable

internuclear separation in the excited states. Since, there is a vibrational energy loss during the life time of excited state and this loss precedes the emission of fluorescence, the energy of fluorescent radiation is, in general, smaller than that of the light initially absorbed. This means that the wavelength of fluorescent light is usually longer than the wave length of light initially absorbed. Through this light emitting process of fluorescence, the absorbed light energy undergoes several decay steps and the light emitting process is spontaneous emission. Thus, even though the illuminating light may be coherent, the spatial distribution of the fluorescence is incoherent and the fluorescence from the object produces fluorescent field that is proportional to the intensity of the incident radiation. Thus fluorescence produces an amount of incoherent light proportional to the intensity of the incident radiation. We can describe the spatial distribution of the fluorescent field by the product of the spatial distribution of fluorescent molecules, $\tau(x, y)$, and the intensity distribution of the illuminating field, $I_s(x, y)$, as

$$I(x, y) = I_s(x, y)\,\tau(x, y), \qquad (2.1-1)$$

where $I(x, y)$ is the intensity distribution of fluorescent light. If the intensity of illuminating light is temporal modulated with a period that is much larger than the fluorescence life-time, the intensity of the fluorescent light varies in correspondence with the intensity of the illuminating light.

$$I_f(x, y, t) = I_s(x, y)cos(wt)\,\tau(x, y), \qquad (2.1-2)$$

where the period of $cos(wt)$ is much smaller than the fluorescence life-time.

3. Optical scanning holography for fluorescent objects in turbid media

Optical scanning holography is an incoherent two dimensional optical scanning method [8,9,10]. The three dimensional holographic information about an object is recorded by two dimensional scanning with a time dependent fresnel zone pattern that is produced by the superposition of a plane wave and a spherical wave at different temporal frequencies.

3.1 Recording stage

A three dimensional intensity pattern created in object space by the superposition of a temporal modulated plane wave and a temporal modulated spherical wave is used to excite the fluorescence of the specimen. Some of the fluorescent light is collected by a detector. The scanning in the transverse plane (x, y) accomplishes a convolution of this pattern with the specimen so that each point-like fluorescent center is encoded in the detector's output in the form of a Fresnel zone pattern having the same transverse coordinate (x, y) as the point object, and a focal length equal to its depth coordinate (z).

3.1.1 Correlation by optical scanning process

Let us consider that the 3-D distribution of the intensity pattern that scans the object plane that is located at $z = z'$ in x, y, z coordinate, as shown in figure 3.1. The intensity of the fluorescent light is proportional to the product of the intensity of the scanning beam and the distribution of fluorescent molecules on the object plane. It is given by

$$I \propto I_s \, \tau, \qquad (3.1.1-1)$$

where I_s is the intensity distribution of the scanning beam and τ is the distribution of fluorescence.

When a 3-D distribution of the intensity pattern (or scanning beam) scans the point (x', y') on object plane in figure 3.1, the intensity of fluorescent light is

$$I(x', y') = \int_{-\infty}^{\infty}\int_{-\infty}^{\infty} I_s(x_1, y_1; z')\, \tau(x_1 + x', y_1 + y'; z')\, dx_1 dy_1, \quad (3.1.1-2)$$

where $I_s(x_1, y_1; z)$ represents the 3-D intensity pattern of scanning beam on object plane. This equation means that when the scanning beam scans on (x', y') point of object plane, the intensity of fluorescent light is proportional to the correlation of scanning beam with object plane at (x', y') point. If we detect the intensity of fluorescent light by photo detector and stored the intensity with the location (x', y') as a form of digital signal, this stored signal will be the correlation of the scanning beam with the object plane (plane of fluorescence molecules).

Let us consider the 3-D distribution of fluorescent molecules (object volume). We can express the object volume as the superposition of the object planes at different location of z with a small interval Δz as shown in figure 3.2 When a 3-D distribution of the intensity pattern (or scanning beam) scans the point (x', y') on the object volume in figure 3.2, the intensity of fluorescent light is the superposition of the fluorescent intensities of each object planes. It is given by

$$I(x', y') = \sum_{m=0}^{n} \Bigg\{ \int_{-\infty}^{\infty}\int_{-\infty}^{\infty} I_s(x_1, y_1; z' + m\,\Delta z) \quad (3.1.1-3)$$

$$\times\, \tau(x_1 + x', y_1 + y'; z' + m\,\Delta z)\, dx_1 dy_1 \Bigg\}.$$

Note that the intensity of the fluorescent light has the information of the interaction of the 3-D intensity pattern of the scanning beam and the 3-D location of fluorescent molecules.

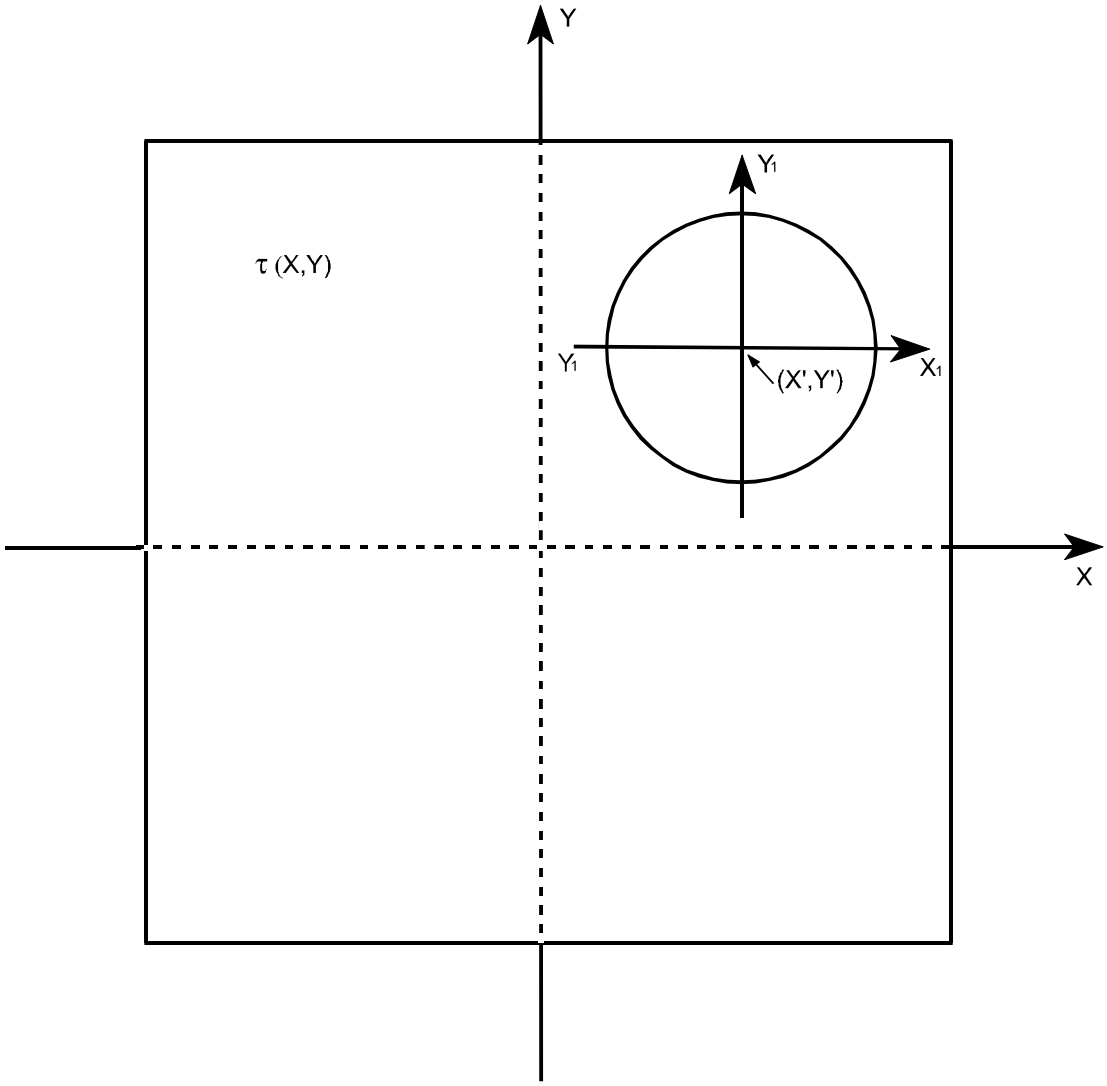

Fig. 3.1 Scanning the object plane located at $z = z'$ by the scanning beam positioned on the object plane ((x', y')plane)

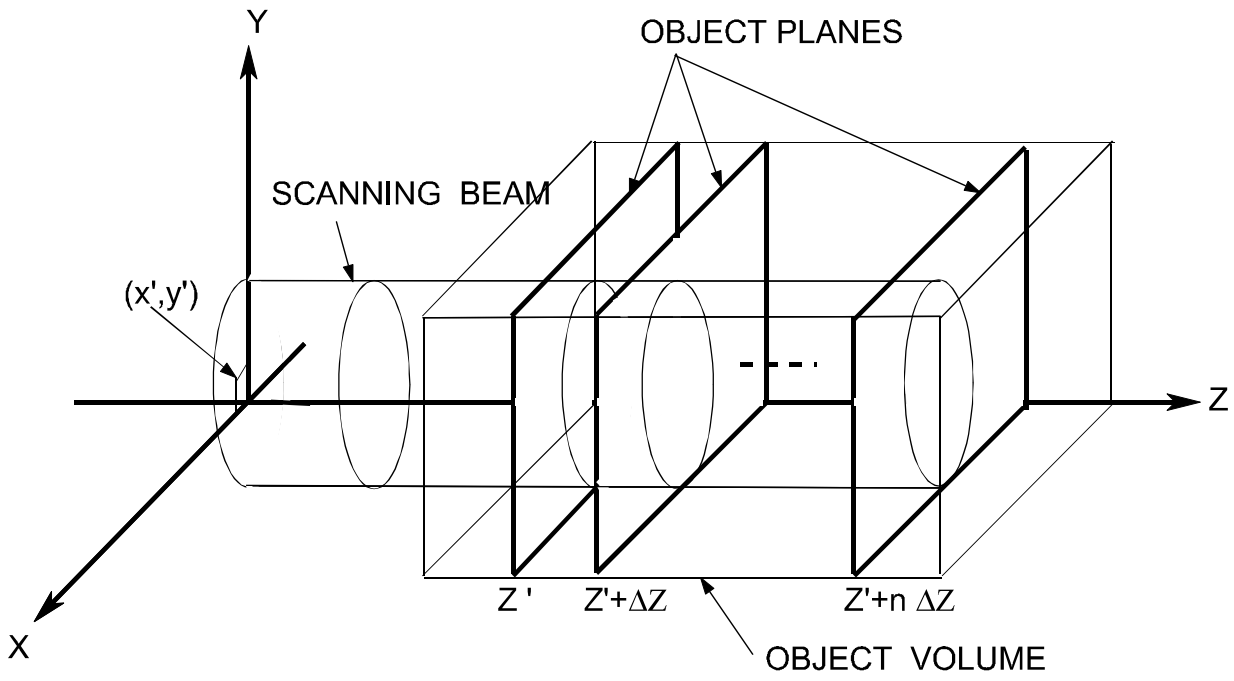

Fig. 3.2 Scanning the object volume by 3-D intensity pattern (scanning beam)

3.1.2 Temporal modulated fresnel zone pattern

Let us consider the optical set up for making a temporal modulated fresnel zone pattern that is used as a 3-D intensity pattern for scanning holography. We generate frequency shifted waves with acousto-optic modulators and make a plane wave and a spherical wave using beam expanders and focusing lens, as shown in figure 3.3.

We produce a fresnel zone pattern by combining the two waves shifted at two different frequencies v_1,v_2 :

$$I_s = \left|U(x_1, y_1; z)exp\Big(- j\,2\pi\, v_1 t\Big) + V(x_1, y_1; z)exp\Big(- j\,2\pi\, v_2 t\Big)\right|^2 \qquad (3.1.2-1)$$
$$= \left|U(x_1, y_1; z)\right|^2 + \left|V(x_1, y_1; z)\right|^2 + Re\{U(x_1, y_1; z)V^*(x_1, y_1; z)exp(\,-j\,2\pi\Delta\, vt)\},$$

where U is a plane wave $\left(U = \frac{j}{\lambda z}exp\big[\,-j\,\frac{2\pi}{\lambda}z\big]\right)$and V is a spherical wave $\left(V = \frac{j}{\lambda z}exp\Big[\,-j\,\frac{2\pi}{\lambda}z - \frac{j\pi(x^2+y^2)}{\lambda z}\Big]\right)$, respectively, and Δv is the temporal frequency difference between the two waves:

$$\Delta v = \left|v_1 - v_2\right|. \qquad (3.1.2-2)$$

Since the real part of the product of the plane wave and the spherical wave forms the fresnel zone pattern, the time dependent term of I_s is the temporal modulated Fresnel zone pattern. The Fresnel zone pattern is ,within a proportionality factor, given by

$$Re\Big\{U(x_1, y_1; z)V^*(x_1, y_1; z)exp\Big(-j\,2\pi\Delta\,vt\Big)\Big\} \qquad (3.1.2-3)$$

$$= cos\Big[\frac{\pi}{\lambda z}\big(x_1^2 + y_1^2\big) + 2\pi\Delta vt\Big]$$

We use this temporal modulated 3-D intensity pattern as a scanning beam because the correlation of this fresnel zone pattern with a fluorescent object generates the hologram of the fluorescent object. In the next section, we will discuss the holographic recording of the fluorescent objects using this 3-D fresnel zone intensity pattern.

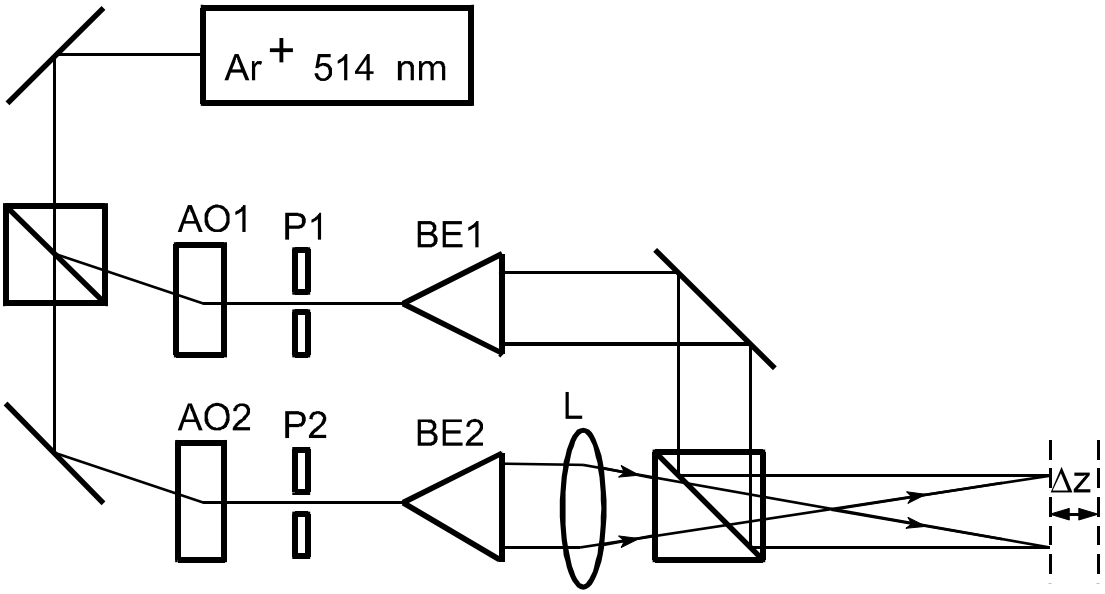

Fig. 3.3 Optical system for making a 3-D intensity pattern for scanning holography (time dependent fresnel zone pattern)

AO1/2	Acousto-optic modulator $(40\,MHz / 40.01\,MHz)$
BE1/2	Beam expander
P1/2	Pin hole aperture
L	Focusing lens

3.1.3 Holographic recording of fluorescent objects by the scanning method

In our optical scanning holographic method, we use the three-dimensional intensity pattern created in the object space by the superposition of a plane wave and a spherical wave at different frequencies for exciting the fluorescent objects. When the period of the temporal modulation of the fresnel zone pattern is much smaller than the life time of the fluorescent object, we can expect the fluorescence to vary temporal in correspondence with the illuminating light (the temporal modulated fresnel zone pattern). Since the Fresnel zone pattern is modulated with a period of $0.1ms$ in our experiment, the intensity of fluorescent light varies temporal with the same period. The output current of the photo detector, termed the heterodyne signal, is the superposition of convolutions of the temporal modulated Fresnel zone pattern and each object planes of fluorescence distribution. Substituting the equation $(3.1.2-1)$ into $(3.1.1-3)$, the output current is given by

$$I = \sum_{m=0}^{n} \Bigg\{ \int_{-\infty}^{\infty}\int_{-\infty}^{\infty} \Big| U(x_1, y_1; z' + m\Delta z) \Big|^2 \qquad (3.1.3-1)$$

$$\tau(x_1 + x, y_1 + y; z' + m\Delta z)\, dx_1 dy_1$$

$$+ \int_{-\infty}^{\infty}\int_{-\infty}^{\infty} \Big| V(x_1, y_1; z' + m\Delta z) \Big|^2$$

$$\tau(x_1 + x, y_1 + y; z' + m\Delta z)\, dx_1 dy_1$$

$$+ \int_{-\infty}^{\infty}\int_{-\infty}^{\infty} cos\Big[\frac{\pi}{\lambda z}\big(x_1^2 + y_1^2\big) + 2\pi\Delta\upsilon t\Big]$$

$$\tau(x_1 + x, y_1 + y; z' + m\Delta z)\, dx_1 dy_1 \Bigg\}$$

After multiplying the heterodyne signal, I with $cos(2\pi\Delta\upsilon t)$ and low pass filtering, we obtain a demodulated signal $i_d(x, y)$:

$$i_d(x, y) = \sum_{m=0}^{n} \Bigg\{ \int_{-\infty}^{\infty}\int_{-\infty}^{\infty} cos\Big[\frac{\pi}{\lambda z}\big(x_1^2 + y_1^2\big)\Big] \qquad (3.1.3-2)$$

$$\tau(x_1 + x, y_1 + y; z' + m\Delta z)\, dx_1 dy_1 \Bigg\}$$

Note that the undesirable space-variant DC terms in equation $(3.1.3-1)$, has been eliminated due to the heterodyne photodetection, and the fluorescent object $\tau(x, y; z)$ has been coded by the cosine Fresnel zone pattern.

When this demodulated signal is displayed on a two-dimensional monitor, we have an image ,or hologram of the object, by a cosine Fresnel zone pattern. This demodulated electric signal can be stored digitally in the computer using analog to digital conversion.

3.2 Reconstruction stage

If we make a transparency of the coded image, we can reconstruct the hologram optically by illuminating it with coherent light and observing the diffraction pattern at some distance, z, away. These diffraction patterns are the reconstructed images at corresponding depth(z). Mathematically, this can be described as the convolution of the coded image with the free space impulse response of light propagation[11] given by

$$h(x,y;z;\lambda) = \frac{j}{\lambda z} exp\left[\frac{-j\pi(x^2+y^2)}{\lambda z}\right]. \qquad (3.2-1)$$

The complex field distribution $f(x,y)$ at a distance z away from the hologram is given by the convolution of the wave emerging from the hologram and $h(x,y;z;\lambda)$ as

$$f(x,y) = \int_{-\infty}^{\infty}\int_{-\infty}^{\infty} i_d(x_1,y_1)h(x-x_1,y-y_1;z;\lambda)dx_1dy_{1.} \qquad (3.2-2)$$

One of the advantages of optical scanning holography is the rejection of the spatially varying bias during recording by the heterodyne process. In standard on-axis holographic recording, this bias acts as noise. Specifically, in standard holographic recording, $|O+R|^2$ is recorded, where O and R represent the wave fronts of the object and the reference

waves, respectively, on the surface of the recording material. We see that $|O+R|^2 = |O|^2 + |R|^2 + OR^* + O^*R,$ where the first two terms are the spatially variant bias recorded in the hologram which produce noise in on-axis holography when the image is reconstructed[14]. These terms cause unnecessary information to be recorded and stored in the hologram. Since this spatially varying bias term is rejected by the heterodyne method in optical scanning holography, we can obtain a higher quality reconstructed image. Since the reconstruction process is linear and space-invariant to same approximation, the digitally stored hologram can also be convolved numerically with a Fresnel zone pattern having a focal length matched to the depth of a chosen plane to be reconstructed. By changing the parameter, $z,$ in the numerical Fresnel zone pattern, we can reconstruct the image of a thick specimen plane by plane, at different depths.

3.3 Selective detection of ballistic photons

When a light wave propagates through a turbid medium, there are two main signal components arriving at a detector [16]: (i) a coherent (ballistic) wave, which arrives first by traveling over the shortest path, and (ii) an incoherent (diffusive) wave which is distorted by random scattering. It is believed that the coherent (ballistic) component of the wave is the least distorted, and the incoherent (diffusive) component of the wave loses most of its shape by random scattering. In our optical scanning holographic system, we extract the ballistic photons to image fluorescent objects in turbid media by using of the temporal and the spatial coherence of ballistic photons. In this section, we will discuss the ballistic photon extraction processes of optical scanning holography. In optical scanning holographic imaging of fluorescent objects in turbid media, there are two stages of ballistic photon extraction process. In the recording stage, ballistic photons are extracted by the heterodyne process, and in the reconstruction stage, diffuse photons are rejected by the holographic selection.

3.3.1 Heterodyne rejection of multiply scattered light in the recording stage

When a light pulse is normally incident upon a semi-infinite region containing random particles as shown in figure 3.4. the transmitted pulse is divided into two parts. One is carried by the ballistic photons and the other is carried by the diffuse photons. The transmitted pulse due to the ballistic photons has the same temporal pulse shape of the incident light because the ballistic photons have little interaction with the scatterers. However, the transmitted pulse carried by the diffuse photons is temporal stretched because of random scattering. The temporal stretching of light pulse carried by the diffuse photons has been analyzed by Akira Ishihmaru [13] and experimentally measured by K. M. Yoo and R. R. Alfano [16].

Let us consider that the temporal impulse light pulse is incident upon a semi-infinite region containing random particles, the temporal stretching profile of the transmitted pulse due to the diffuse photons derived by Akira Ishimaru is given by

$$h_d(t) \propto exp(-\alpha t)\, ln\left(\frac{1}{1-\frac{\Delta t}{t}}\right) step(t-\Delta t), \qquad (3.3.1-1)$$

where α represents the temporal stretching coefficient of diffuse photons, Δt is the time that is needed to pass through the turbid medium and $step(t)$ represents the step function. The profile of the temporal stretching is shown in figure 3.5. For mathematical simplicity, we assume that the temporal profile of stretched pulse is a one-sided exponential function, $\frac{1}{T} exp\left[\frac{-(t-\Delta t)}{T}\right] step(t-\Delta t)$, where T represents the temporal duration of the time stretching as shown in figure 3.5.

When temporal modulated Fresnel zone pattern is incident upon a semi-infinity region containing random particles as shown in figure 3.3, the temporal response to the Fresnel zone pattern is composed of two part. One part of response due to the ballistic photons and this has a same temporal profile of incident Fresnel zone pattern. The other part of response due to the diffuse photons is temporal distorted and the temporal distorted pattern of temporal modulated Fresnel zone pattern can be expressed by the convolution of temporal modulated Fresnel zone pattern and impulse response of light pulse carried by the diffuse photons. Thus the Fresnel zone pattern carried by the diffuse photons can be expressed as:

$$FZP_{df}(x,y;z) = cos\Big[\frac{\pi}{\lambda z}(x^2+y^2) + 2\pi\Delta\upsilon t\Big] \qquad (3.3.1-2)$$
$$*\frac{1}{T}\, exp\Big[\frac{-(t-\Delta t)}{T}\Big] step(t-\Delta t)\,,$$

where FZP_{df} represents temporal distorted Fresnel zone pattern due to the diffuse photons and $*$ represents temporal convolution.

$cos\big[\frac{\pi}{\lambda z}(x^2+y^2) + 2\pi\Delta\upsilon t\big] * \frac{1}{T} exp\Big[\frac{-(t-\Delta t)}{T}\Big] step(t-\Delta t)$ is expressed, in Fourier domain, by

$$\begin{aligned} &\Big\{\frac{1}{2}exp\Big[j\frac{\pi}{\lambda z}(x^2+y^2)\Big]\delta(f-\Delta\upsilon) \qquad (3.3.1-3)\\ &+\frac{1}{2}exp\Big[-j\frac{\pi}{\lambda z}(x^2+y^2)\Big]\delta(f+\Delta\upsilon)\Big\}\frac{exp(-j2\pi f\Delta t)}{1+j2\pi fT}\\ &=\Big\{\frac{1}{2}exp\Big[j\frac{\pi}{\lambda z}(x^2+y^2)\Big]\delta(f-\Delta\upsilon)\\ &+\frac{1}{2}exp\Big[-j\frac{\pi}{\lambda z}(x^2+y^2)\Big]\delta(f+\Delta\upsilon)\Big\}\frac{exp(-j2\pi f\Delta t)}{1+j2\pi\Delta\upsilon T} \end{aligned}$$

Therefore, the temporal distorted Fresnel zone pattern by the diffuse photons is given by

$$cos\Big[\frac{\pi}{\lambda z}(x^2+y^2)+2\pi\Delta\upsilon t\Big]*\frac{1}{T}exp\Big[\frac{-(t-\Delta t)}{T}\Big]step(t-\Delta t) \qquad (3.3.1-4)$$

$$=\frac{1}{1+j2\pi\Delta\upsilon T}cos\Big[\frac{\pi}{\lambda z}(x^2+y^2)+2\pi\Delta\upsilon(t-\Delta t)\Big]$$

Let us consider the amplitude of the temporal modulated Fresnel zone pattern carried by the diffused photons. The amplitude of temporal modulated Fresnel zone pattern carried by diffused photons is given by

$$A_{td}=\left|\frac{1}{1+j2\pi\Delta\upsilon T}\right| \qquad (3.3.1-5)$$

$$=\left|\frac{1}{(1+4\pi^2\Delta\upsilon^2T^2)^{\frac{1}{2}}}\right|$$

where A_{td} represents the amplitude of temporal modulated Fresnel zone pattern carried by the diffuse photons.

Note that if $\Delta\upsilon\geq\frac{1}{2\pi T}$, A_{td} is smaller than $\frac{1}{2}$. Comparing to the incident amplitude of Fresnel zone pattern, the amplitude of Fresnel zone pattern carried by the diffuse photons is reduced to half of the amplitude of the incident Fresnel zone pattern. This means that more than half of diffuse photons are rejected when we modulate Fresnel zone pattern at frequency of $\Delta\upsilon\geq\frac{1}{2\pi T}$. Since the temporal profile of temporal modulated Fresnel zone pattern by the diffuse photons is temporal distorted by the temporal stretching of the diffuse photons, the distorted Fresnel zone pattern by diffuse photons is

rejected in heterodyne process. In addition to temporal distortion of Fresnel zone pattern carried by the diffuse photons, the Fresnel zone pattern is distorted spatially also. Therefore, the Fresnel zone pattern, by diffuse photons, can not maintain its shape in turbid medium. If we assume that only the phase of Fresnel zone pattern is distorted, the output current of photo detector by the Fresnel zone pattern carried by the diffuse photons is expressed by

$$I = \int_{-\infty}^{\infty}\int_{-\infty}^{\infty} cos\Big[\frac{\pi}{\lambda z}(x^2+y^2) + 2\pi\Delta\upsilon t + \Delta\theta\Big] \qquad (3.3.1.-6)$$

$$\tau(x_1+x, y_1+y; z)\, dx_1\, dy_1,$$

where $\Delta\theta$ is the phase distortion due to the diffuse photons.

After multiplying the heterodyne scanned signal, I, with $cos(2\pi\Delta\upsilon t)$ and passing through a low pass filter, we have a demodulated signal $i_d(x,y)$:

$$i_d(x,y) = \Bigg[\int_{-\infty}^{\infty}\int_{-\infty}^{\infty} cos\Big[\frac{\pi}{\lambda z}(x^2+y^2)\Big] \qquad (3.3.1-7)$$

$$\times\, \tau(x_1+x, y_1+y; z) dx_1 dy_1\Bigg] cos(\Delta\theta).$$

Note that, since $\Delta\theta$ is a phase distortion by random scattering, this can have any values between 0 to 2π. If we assume that the phase distortion is equally probable, in other word, $\Delta\theta$ has a uniform probability distribution between 0 to 2π, and if scanning time is long enough for many changes of random phase to occur, the average power of out put current of photo detector is given by

$$< i_d^2 > = \left[\int_{-\infty}^{\infty}\int_{-\infty}^{\infty} cos\Big[\frac{\pi}{\lambda z}(x^2+y^2)\Big]\tau(x_1+x, y_1+y; z)dx_1dy_1\right]^2 \quad (3.3.1-8)$$

$$\times \frac{1}{2\pi}\int_0^{2\pi} cos^2(\Delta\theta)d\Delta\theta$$

$$= \frac{1}{2}\left[\int_{-\infty}^{\infty}\int_{-\infty}^{\infty} cos\Big[\frac{\pi}{\lambda z}(x^2+y^2)\Big]\tau(x_1+x, y_1+y; z)dx_1dy_1\right]^2$$

Note that, comparing to the original signal power of Fresnel zone pattern $\left(\left[\int_{-\infty}^{\infty}\int_{-\infty}^{\infty} cos\big[\frac{\pi}{\lambda z}(x^2+y^2)\big]\tau(x_1+x, y_1+y; z)dx_1dy_1\right]^2\right)$, the signal power of Fresnel zone pattern carried by the diffused photons is reduced to half of the signal power. This means that through the demodulation in the heterodyne process, half of the Fresnel zone pattern carried by the diffuse photons is rejected. In heterodyne process of optical scanning holographic method, the Fresnel zone pattern carried by diffused photons is rejected because the Fresnel zone pattern carried by the diffuse photons lose its temporal coherence with source due to the temporal stretching of diffuse photons and the random varying of light phase and in heterodyne process, only the signal having the coherence with source is selectively detected.

3.3.2 Holographic rejection of multiply scattered light in the reconstruction stage

When a Fresnel zone pattern is normally incident upon a semi-infinite region containing random particles as shown in figure 3.4, there exists a 3-D intensity pattern, in the turbid medium, that is composed of two parts. One part is the image carried by the ballistic photons and the other part is the image carried by the diffused photons. Ballistic photons are unscattered or are scattered only few times, these photons retain some correlation with the source, and therefore, the image from the ballistic photons retains the shape of the Fresnel zone pattern. However, the image carried by the diffused photons loses its shape. If we assume that the Fresnel zone pattern is distorted spatially and not distorted temporal, the 3-D intensity pattern in the turbid medium can be expressed as

$$FZP = cos\left[\frac{\pi}{\lambda z}\left(x^2 + y^2\right) + 2\pi\Delta\upsilon t\right] + S_d(x, y; z)cos(2\pi\Delta\upsilon t), \qquad (3.3.2-1)$$

where $S_d(x, y)$ is the distorted part by random scattering.

The output current of photo detector is given by the convolution of 3-D intensity pattern with the distribution of the fluorescent molecules, $\tau(x, y; z)$. Thus the output current is given by

$$I(x, y) = \int_{-\infty}^{\infty}\int_{-\infty}^{\infty} cos\left[\frac{\pi}{\lambda z}\left({x_1}^2 + {y_1}^2\right) + 2\pi\Delta\upsilon t\right] \tau(x_1 + x, y_1 + y; z\,) \quad (3.3.2-2)$$
$$+ S_d(x_1, y_1; z)\tau(x + x_1, y + y_1; z)cos(2\pi\Delta\upsilon t)dx_1 dy_1$$

After multiplying the heterodyne scanned signal, I, with $cos(2\pi\Delta\upsilon t)$ and passing through a low pass filter, we have a demodulated signal:

$$i_d(x,y) = \int_{-\infty}^{\infty}\int_{-\infty}^{\infty} cos\Big[\frac{\pi}{\lambda z}\big(x_1^2 + y_1^2\big)\Big]\tau(x_1 + x, y_1 + y; z)dx_1dy_1 \quad (3.3.2-3)$$

$$+ \int_{-\infty}^{\infty} S_d(x_1, y_1; z)\tau(x + x_1\,, y + y_1; z)\, dx_1dy_1$$

Note that the term $\int_{-\infty}^{\infty} S_d(x_1, y_1; z)\tau(x + x_1\,, y + y_1; z)\, dx_1dy_1$ cannot contribute to form a hologram because $S_d(x, y; z)$ loses the shape of the Fresnel zone pattern by random scattering. Therefore, in the reconstruction process, the $S_d(x, y; z)*\tau(x, y; z)$ term is rejected as background noise. The physical process in the holographic rejection is that when the Fresnel zone pattern is scattered by scatterers, the spatially distorted Fresnel zone pattern cannot form interference fringes with the fluorescent objects; thus only the Fresnel zone pattern carried by ballistic photons contribute to form the hologram. Through these diffused photon rejection processes, we can successfully extract ballistic photons and make the 3-D image of the fluorescent objects in turbid media. These diffused photons rejection processes are experimentally verified in section 3.4.

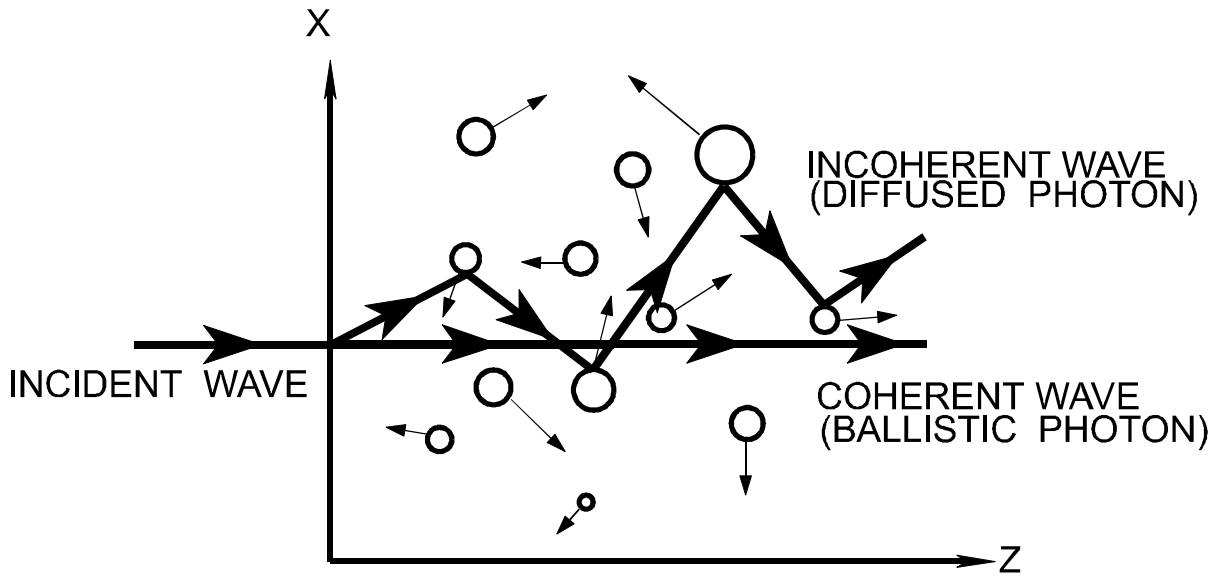

Fig. 3.4 Coherent and incoherent waves propagate through a turbid media

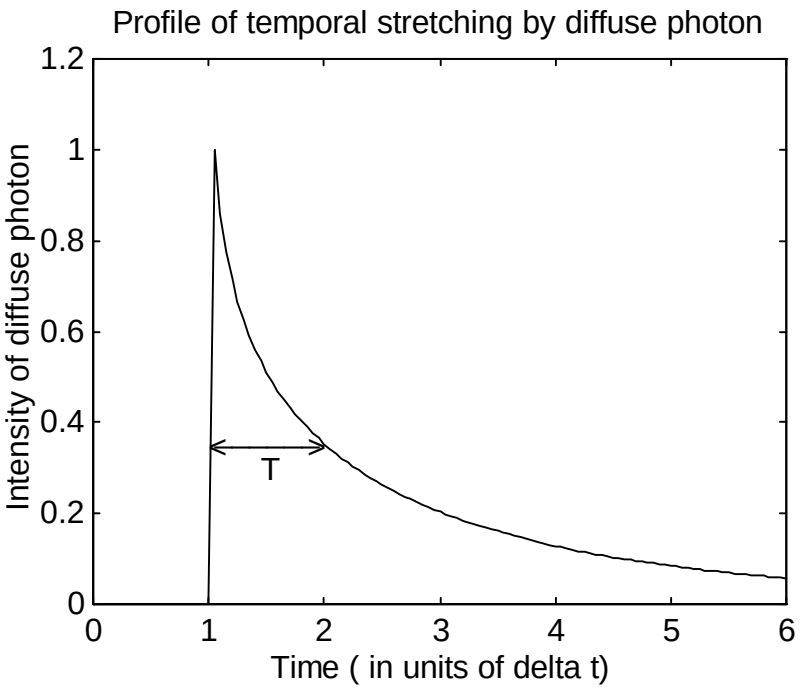

Figure 3.5 Profile of temporal stretching by diffused photon

3.4 Electronic multiplexing method for eliminating twin-image noise in optical scanning holography

The optical scanning holographic record is a coding of a 3-dimensional object with an intensity pattern of a temporal modulated Fresnel zone pattern. There is undesirable defocused twin image noise, as in conventional in-line holography. In this chapter, we review the multiplexing method [10] for eliminating twin image noise in optical scanning holography. We realize the proposed multiplexing method [10].

3.4.1 Origin of the twin image

When the hologram is reconstructed by a laser with wavelength λ_o, or numerically reconstructed by the convolution of a numerical Fresnel zone pattern that has a certain focal length, a real image and a virtual image will be formed simultaneously at distance z in front and in back of the hologram, respectively, both images being centered on the hologram axis. The twin image acts as a defocused image noise in digital reconstruction because the reconstruction is focused on either $+z$ and $-z$. To understand the origin of the formation of the twin-image, we expand the cosine term in $(3.1.3-2)$ as

$$cos\Big[\frac{\pi}{\lambda z}(x_1^2+y_1^2)\Big] \qquad (3.4.1-1)$$

$$= \frac{1}{2}\Big[exp\Big(j\frac{\pi}{\lambda z}(x_1^2+y_1^2)\Big) + exp\Big(-j\frac{\pi}{\lambda z}(x_1^2+y_1^2)\Big)\Big].$$

In equation $(3.4.1-1)$, we can observe the complex conjugated exponential function pair. This pair of exponential terms generate the pair of reconstructed image at $+z$ and $-z$. The first exponential in $(3.4.1-1)$ is responsible for the reconstruction of a real-image,

whereas the second exponential term produces the twin image that generates unwanted noise on the real image reconstruction plane.

3.4.2 Multiplexing method to eliminate twin image noise in optical scanning holography [14]

We create the cosine Fresnel zone pattern through the following process. First, the object is scanned using a time dependent Fresnel zone pattern, which produces a heterodyne current and then the heterodyne current is subsequently multiplied by $cos[2\pi\Delta vt\ ]$ and low-pass filtered, giving rise to a cosine Fresnel zone pattern coded image given by $(3.1.3-2)$. If we multiply the current by $sin[\ 2\pi\Delta vt\ ]$simultaneously and do low-pass filtering, we get the sine Fresnel zone pattern coded holographic record that is given by

$$i_d^Q(x,y) = \int_{-\infty}^{\infty}\int_{-\infty}^{\infty} sin\Big[\frac{\pi}{\lambda z}\big(x_1^2+y_1^2\big)\ \Big] \qquad (3.4.2-1)$$

$$\tau(x_1+x, y_1+y; z)\, dx_1 dy_1.$$

We call i_d^Q the sine Fresnel zone pattern coded holographic record and i_d the cosine Fresnel zone pattern coded holographic record. Now we can add $i_d^Q(x,y)$ and $i_d\ (x,y)$ to form a complex scanned signal as

$$i_c(x,y) = i_d(x,y) + j\, i_d^Q(x,y) \qquad (3.4.2-2)$$

$$= \int_{-\infty}^{\infty}\int_{-\infty}^{\infty} exp\Big[j\frac{\pi}{\lambda z}\big(x_1^2 + y_1^2\big)\ \Big]\tau(x_1 + x, y_1 + y; z)\, dx_1 dy_1$$

Note that since equation $(3.4.2-2)$ is only composed of a single exponential term, $i_c(x(t), y(t))$ is a single side band holographic record of $\tau(x, y; z)$, which will only give rise to the real image upon reconstruction. This concept of simultaneous acquisition of the cosine- and sine- coded images is called the multiplexing method [10]. The set up realizing this is shown in figure 3.6. The signal I obtained from the output of photo detector is simultaneously multiplied by $cos[2\pi\Delta vt\ ]$ and $sin[2\pi\Delta vt\ ]$ to obtain $i_d(x(t), y(t))$ and $i_d^Q(x(t), y(t))$, respectively. The complex addition of $i_d(x(t), y(t))$, according to $(4.2-2)$, is performed digitally by a personal computer (PC).

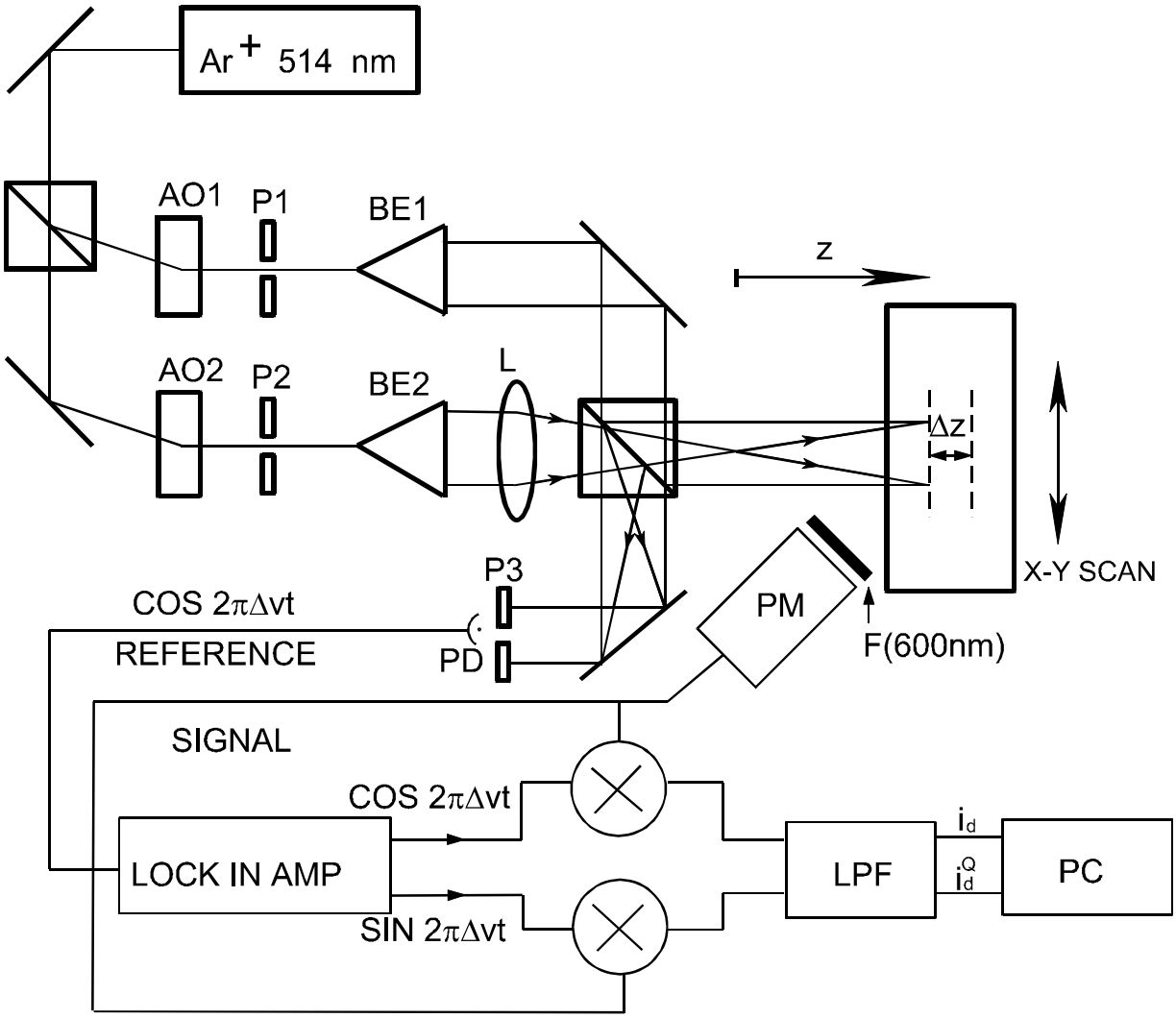

Fig. 3.6. Optical set up for acquiring cosine and sine coded images simultaneously

BE1/2 Beam expander
P1/2 Pin Hole aperture
L Focusing Lens
PD Photo diode
PM Photo multiplier
F Fluorescence filter
i_d/i_d^Q In phase (cosine) and quadrature (sine) holographic signals
LPF Low pass filter
PC : Personal computer

3.4.3 Experimental results

The optical set up is shown in figure 3.6. The excitation field is a Fresnel zone pattern resulting from the interference of a plane wave and a co-directional spherical wave (formed by lens L) from an Argon-ion laser $(514\,nm)$, and with a frequency difference of $10\,KHz$. This was achieved by placing an acousto-optic modulator in each arm of the interferometer, shown in figure 3.6, and driving each arm coherently at $40MHz$ and 40.01 MHz respectively. At the specimen location, the spherical wave has a radius of curvature $z \sim 8cm$, as shown in figure 3.6, and the Fresnel zone pattern has a numerical aperture $NA \sim 0.01$. The expected transverse resolution and depth of field are thus $\Delta x \sim 50\ \mu m$; $\Delta z \sim 5\ mm$ respectively. In the experiment, however, aberrations and distortions of the Fresnel zone pattern, together with the bandwidth limitation of the detection system contribute to reducing the effective numerical aperture, spoiling the transverse resolution and reducing sizably the depth discrimination. These factors could be improved by a better system design. The fluorescent light modulated at $10\,KHz$ is collected by a photomultiplier through a narrow band filter centered at $600nm$ to reject the $514nm$ laser light. The detector has a diameter of $\sim 1cm$ and is placed in front of the specimen, as shown in figure 3.6. A phase sensitive amplifier demodulates the signals, which are digitized and stored to produce a holographic record. The reference for demodulation comes from the same modulated interference pattern that scans the sample and is picked up at the second part of the beam splitter (figure 3.6). This insures that phase fluctuations and drifts due to possible interferometric instabilities are to a great extent canceled out.

The specimen consists of two hollow core optical fibers (inner/outer diameter ~ 120 $\mu m/400\,\mu m$) stripped of their coating and filled with $Rhodamine\,6G$ ($1g/1$ in methanol). The two fibers are $\Delta x \sim 1mm$ apart transversally, and $\Delta z \sim 12\ mm$ apart axially. The fibers are immersed in a $4\,cm$ deep cuvette with the front fiber about $8mm$ behind the entrance window of the cuvette. The turbid medium is a water solution of

polystyrene beads ($0.18\,\mu m$ diameter, 10 % solid), for which an extinction coefficient $\mu \sim 2.8(cm\%Vol)^{-1}$ was measured at $514\,nm$. At the concentration $\sim 0.25\%Vol.$ used in the first experiment shown, the extinction length was measured as $l \sim 1.5\,cm$, assuming a beer's extinction law of the form $I/I_o \sim exp(-z/l)$. Figure 3.7 shows the holographic record for a one line scan along the x cross of the specimen. Figure 3.8 shows the line reconstruction at two different depths. The first trace is focused on the front fiber; the second is focused on the back fiber at a distance of $\sim 12mm$ from the front one. Figure 3.9 shows a contour plot of the intensity in the $x-z$ plane, from which the locations of the two fluorescent fibers can be quantitatively determined. As expected, the reconstruction of the sample embedded deeper in the turbid medium is considerably weaker, for three obvious reasons: The scanning Fresnel zone pattern has to penetrate farther in the medium; the fluorescent light is scattered on its way back through the medium toward the detector, and the sample is farther away from the detector. In principle, once the various fluorescent centers of the sample have been approximately located, it is possible to compensate a posterior for these effects by using suitable image processing methods. With certain types of objects, approximate 3-D location information could also be extracted directly from the hologram, using e.g., Wigner analysis [9]. In fact, once the hologram is recorded, a number of image processing algorithms and techniques can be used to manipulate the 3-D reconstruction at will. To better estimate the capacity of the method, Figure 3.10 shows the reconstruction of a fiber embedded $\sim 30mm$ behind the entrance window of the cuvette. Here, the turbid medium concentration was increased to $\sim 0.6\%Vol.$, corresponding to a measured extinction length $l \sim 6\,mm$. The obvious limitation is due to the large, noisy background. Its presence could be traced to modulated laser light leaking through the imperfect (rejection ratio $\sim 10^{-3}$) interference filter used to select the yellow fluorescent light. No attempt was made to filter out the noise, either directly or a posterior.

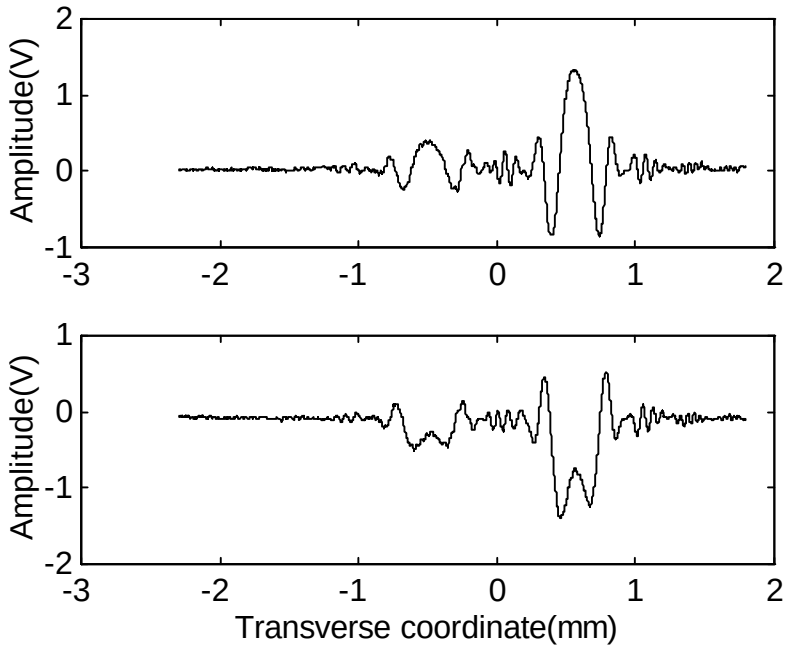

Fig. 3.7 Trace through the holographic record, up: cosine hologram, down: sine hologram

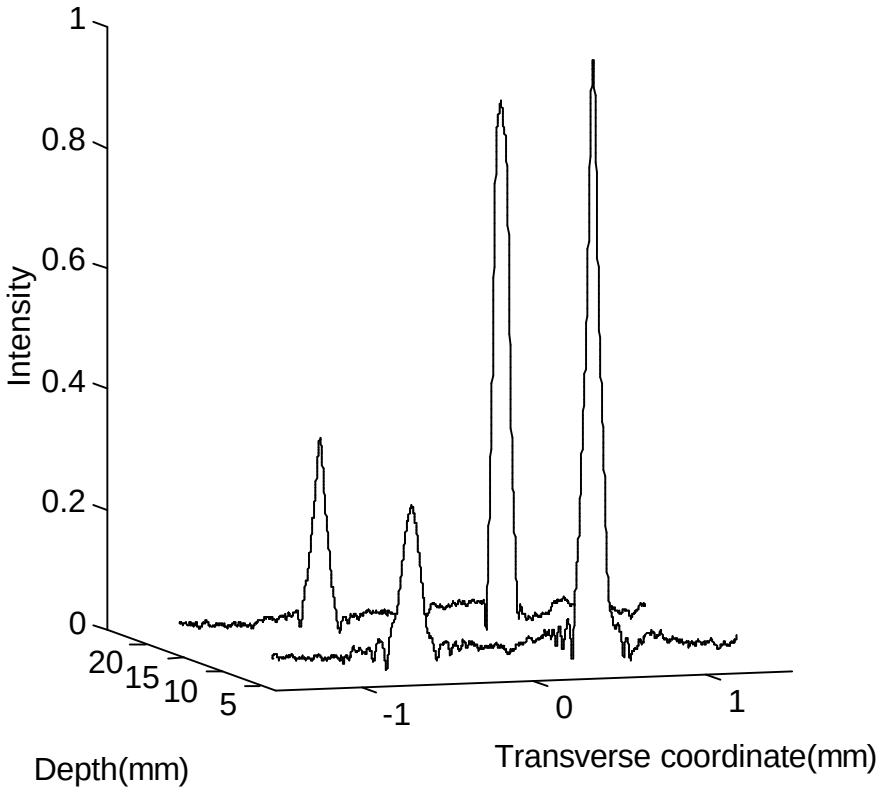

Fig. 3.8 Traces through the reconstruction of two hollow core fibers ($120\,\mu m$ inner diameter) filled with $Rhodamine\,6G$ embedded $8mm$ and $20mm$ respectively behind the cuvette window. The turbid medium is a water solution of polystyrene beads with an extinction length $\sim 15mm$. The two fibers are $\Delta x \sim 1mm$ and $\Delta z \sim 12mm$ apart. Each trace is focused on a different fiber.

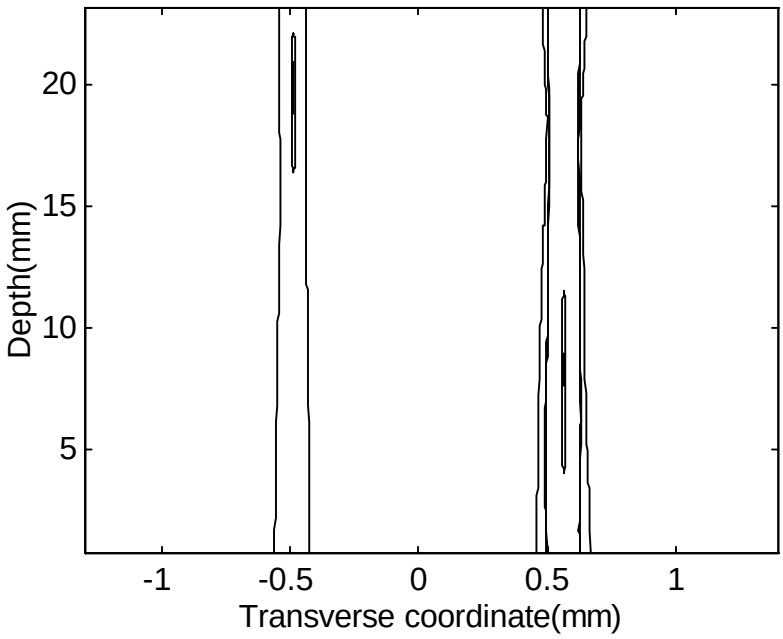

Fig. 3.9 Contour plot of the intensity in a $x - z$ plane through the reconstruction, allowing the quantitative location of the two fibers

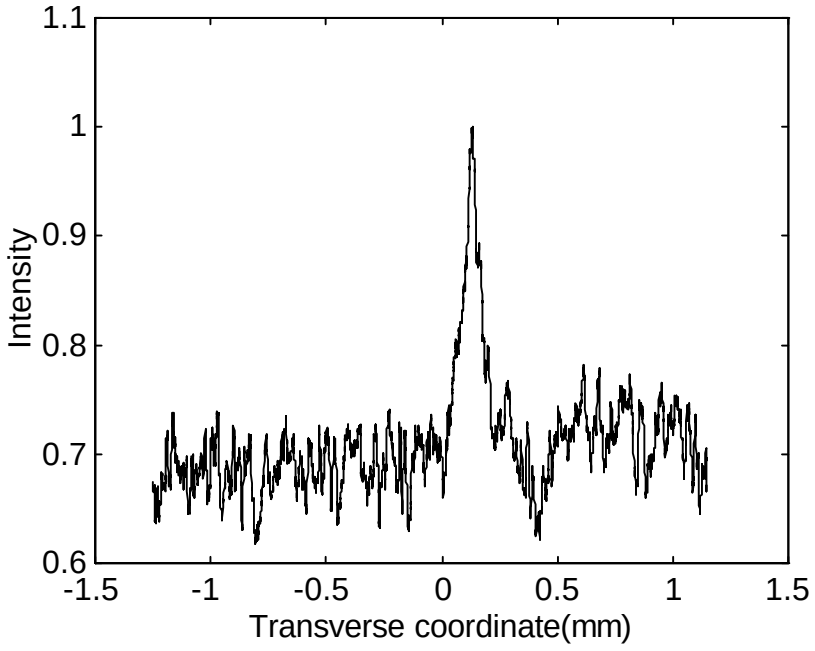

Fig. 3.10 Reconstruction of a hollow core fiber embedded $30mm$ behind the cuvette window with a turbid medium having an extinction length $\sim 6mm$.

Chapter 4 Adjusted digital filter for twin image elimination

In this chapter, we review a recursive filtering algorithm designed to decode the fluorescent object $(\tau(x, y; z))$ directly from the cosine hologram (i_d) without the presence of the twin image noise [15]. This digital decoding method is first proposed by L. Onural and Peter D.Scott [15]. The principal achievement of this filter is the suppression of twin image noise without an additional physical set up because the filtering operation is performed completely by digital means. However, because the frequency of filter increases geometrically as the loop continues, in digital realization of this filter, the aliasing noise problem occurs. In order to overcome this aliasing noise problem, I propose the adjusted digital filtering algorithm, in which the filter reduces its size to satisfy the Nyquist sampling criteria.

4.1 Digital decoding of holograms [15]

From the equation $(3.2-1)$, we can say that the holographic recording can be modeled as a simple linear shift invariant 2-D system.

$$i_d(x(t), y(t)) = \int_{-\infty}^{\infty}\int_{-\infty}^{\infty} cos\Big[\frac{\pi}{\lambda z}\big(x_1^2 + y_1^2\big)\Big] \qquad (4.1-1)$$

$$\tau(x_1 + x, y_1 + y; z)\, dx_1 dy_1$$
$$= \tau(x, y; z) * j\lambda z\{\, Re[h_z(x, y)\,]\}$$

where $h_z(x, y) = \frac{1}{j\lambda z} exp\big[j\frac{\pi}{\lambda z}(x^2 + y^2)\big]$ is the free space impulse response of the holographic recording system, and $*$ represents convolution.

Since the convolution of each component with itself or the convolution between the real component and the imaginary component of this impulse response produce the following recursive relation with the impulse response, we can reconstruct the original image by filtering out the twin image by the use of the following recursive relationship:

$$Im\{h_z\}*Im\{h_z\} = \frac{1}{2}\delta(x,y) - \frac{1}{2}Re\{h_{2z}\} \qquad (4.1-2)$$

$$Re\{h_z\}*Re\{h_z\} = \frac{1}{2}\delta(x,y) + \frac{1}{2}Re\{h_{2z}\} \qquad (4.1-3)$$

$$Im\{h_z\}*Re\{h_z\} = \frac{1}{2}Im\{h_{2z}\} \qquad (4.1-4)$$

The auto convolution of the imaginary parts of the impulse response at z results in a delta function minus the real part of free space impulse response at twice the distance. The auto convolution of the real part of the free space impulse response results in delta function plus the real part of free space impulse response at twice the distance. The convolution of the imaginary part of the impulse response with its real part results in the imaginary part of the impulse response at twice the distance. By the use of these recursive relationships, we can define the following recursive algorithm to extracts the real image.

Initial step

$$I*Re\{h_z\} = P_o = 1 + \frac{1}{2}\tau + \frac{1}{2}\tau*Re\{h_{2z}\} \qquad (4.1-5)$$

Second step

$$I*Im\{h_z\} = S_1 = \tau*\tfrac{1}{2}Im\{h_{2z}\} \qquad (4.1-6)$$
$$S_1*2Im\{h_{2z}\} = P_1 = \tfrac{1}{2}\tau - \tfrac{1}{2}\tau*Re\{h_{4z}\}$$

Recursive step

$$S_n*2Re\{h_{2^n z}\} = S_{n+1} = \tau*\tfrac{1}{2}Im\{h_{2^{n+1} z}\} \qquad (4.1-7)$$
$$S_{n+1}*2Im\{h_{2^{n+2} z}\} = P_{n+1} = \tfrac{1}{2}\tau - \tfrac{1}{2}\tau*Re\{h_{2^{n+3} z}\}$$

where n is the number of loops.

Let us sum up all P_n to $n = M$

$$\tau_r = \frac{2}{M}\left\{\sum_{n=0}^{M} P_n\right\} \qquad (4.1-8)$$

$$= \frac{2}{M}\left\{1 + \frac{1}{2}(M+1)\,\tau - \frac{1}{2}\,\tau * \left[Re\{h_{2z}\} - \sum_{n'=1}^{M} Re\{h_{2^{n'+1} z}\}\right]\right\}$$

When the number of loops goes to infinity, the filtered image(τ_r) approaches the reconstructed image(τ_r) without twin image noise.

$$\tau_r = \lim_{M\to\infty}\left[\frac{2}{M}\left\{\sum_{n=0}^{M} P_n\right\}\right] \qquad (4.1-9)$$

$$= \lim_{M\to\infty}\left[\frac{2}{M} + \tau + \frac{1}{M}\tau - \frac{1}{M}\,\tau * \left[Re\{h_{2z}\} - \sum_{n'=1}^{M} Re\{h_{2^{n'+1}z}\}\right]\right]$$

$$= \tau - \lim_{M\to\infty}\left\{\tfrac{1}{M}\,\tau * \left[Re\{h_{2z}\} - \sum_{n'=1}^{M} Re\{h_{2^{n'+1}z}\}\right]\right\}$$

In equation $(4.1-9)$, if the residue term, $\lim_{M\to\infty}\left\{\tfrac{1}{M}\,\tau * \left[Re\{h_{2z}\} - \sum_{n'=1}^{M} Re\{h_{2^{n'+1}z}\}\right]\right\}$ goes to zero, then the filtered image becomes the reconstructed image without twin image noise.

When the number of loop goes to infinity, the residue term is given by

$$\lim_{M\to\infty}\left\{\frac{1}{M}\,\tau * \left[Re\{h_{2z}\} - \sum_{n'=1}^{M} Re\{h_{2^{n'+1}z}\}\right]\right\} \qquad (4.1-10)$$

$$= \tau * \lim_{M\to\infty}\left\{\frac{1}{M}\left[Re\{h_{2z}\} - \sum_{n'=1}^{M} Re\{h_{2^{n'+1}z}\}\right]\right\}$$

$$= \tau * \lim_{M\to\infty}\left\{\frac{1}{M}\left[sin\frac{\pi}{\lambda z}(x^2+y^2) - \sum_{n'=1}^{M}\frac{1}{2^{n'+1}} sin\frac{\pi}{2^{n'+1}\lambda z}(x^2+y^2)\right]\right\}$$

Since λ, z, x are real values, $sin\frac{\pi}{\lambda z}(x^2+y^2)$ in equation $(4.1-10)$ is bounded by

$$-1 \leq sin\frac{\pi}{\lambda z}\left(x^2+y^2\right) \leq 1 \qquad (4.1-11)$$

$\frac{1}{2^{n'+1}}$ is a positive real value, thus $\frac{1}{2^{n'+1}}\ sin\frac{\pi}{2^{n'+1}\lambda z}(x^2+y^2)$ is also bounded

$$-\ \frac{1}{2^{n'+1}} \leq\ \frac{1}{2^{n'+1}} sin\frac{\pi}{2^{n'+1}\lambda z}\left(x^2+y^2\right) \leq\ \frac{1}{2^{n'+1}} \qquad (4.1-12)$$

Since each component of the summation is bounded, the summation of the above component is bounded also.

$$-\sum_{n'=1}^{M}\frac{1}{2^{n'+1}} \leq \sum_{n'=1}^{M}\frac{1}{2^{n'+1}} sin\frac{\pi}{2^{n'+1}\lambda z}\left(x^2+y^2\right) \leq \sum_{n'=1}^{M}\frac{1}{2^{n'+1}} \qquad (4.1-13)$$

Since $\sum_{n'=1}^{M}\frac{1}{2^{n'+1}}$ is the summation of a geometric series, it is given by

$$\sum_{n'=1}^{M}\frac{1}{2^{n'+1}} = \frac{\frac{1}{4}(1-\left(\frac{1}{2}\right)^M}{1-\frac{1}{2}} \qquad (4.1-14)$$

$$= \frac{1}{2}\left(1-\left(\frac{1}{2}\right)^M\right)$$

Using equation$(4.1-14)$ into equation$(4.1-13)$.

$$-\frac{1}{2}\left(1-\left(\frac{1}{2}\right)^{M}\right) \leq \sum_{n'=1}^{M} \frac{1}{2^{n'+1}} sin \frac{\pi}{2^{n'+1}\lambda z}\left(x^2+y^2\right) \qquad (4.1-15)$$

$$\leq \frac{1}{2}\left(1-\left(\frac{1}{2}\right)^{M}\right)$$

When M goes to infinity, $-\frac{1}{2}\left(1-\left(\frac{1}{2}\right)^{M}\right)$ goes to $\frac{1}{2}$. Thus, when M goes to infinity, $\sum_{n'=1}^{M} \frac{1}{2^{n'+1}} sin \frac{\pi}{\lambda z}(x^2+y^2)$ is bounded:

$$-\frac{1}{2} \leq \sum_{n'=1}^{\infty} \frac{1}{2^{n'+1}} sin \frac{\pi}{2^{n'+1}\lambda z}\left(x^2+y^2\right) \leq \frac{1}{2} \qquad (4.1-16)$$

Thus $sin \frac{\pi}{\lambda z}(x^2+y^2) + \sum_{n'=1}^{\infty} \frac{1}{2^{n'+1}} sin \frac{\pi}{\lambda z}(x^2+y^2)$is bounded also. The residue term is bounded by

$$-\frac{3}{2M} \leq \frac{1}{M}\left\{sin \frac{\pi}{\lambda z}(x^2+y^2) + \sum_{n'=1}^{\infty} \frac{1}{2^{n'+1}} sin \frac{\pi}{2^{n'+1}\lambda z}(x^2+y^2)\right\} \qquad (4.1-17)$$
$$\leq \frac{3}{2M}$$

When M goes to infinity, $-\frac{3}{2M}$ and $\frac{3}{2M}$ goes to zero and $\frac{1}{M}\left\{sin \frac{\pi}{\lambda z}(x^2+y^2) + \sum_{n'=1}^{\infty} \frac{1}{2^{n'+1}} sin \frac{\pi}{2^{n'+1}\lambda z}(x^2+y^2)\right\}$ is bounded by $-\frac{3}{2M}$ and $\frac{3}{2M}$.

Hence

$$\lim_{M\to\infty} \frac{1}{M}\left\{ sin\frac{\pi}{\lambda z}(x^2+y^2) + \sum_{n'=1}^{\infty} \frac{1}{2^{n'+1}} sin\frac{\pi}{2^{n'+1}\lambda z}(x^2+y^2) \right\} \qquad (4.1-18)$$
$$= 0$$

Thus the residual term in equation $(4-9)$ goes to zero. Therefore, as M goes to infinity, the reconstructed image is the original image without twin image noise:

$$\tau_r = \tau \qquad (4.1-19)$$

The algorithm is summarized in figure 4.1

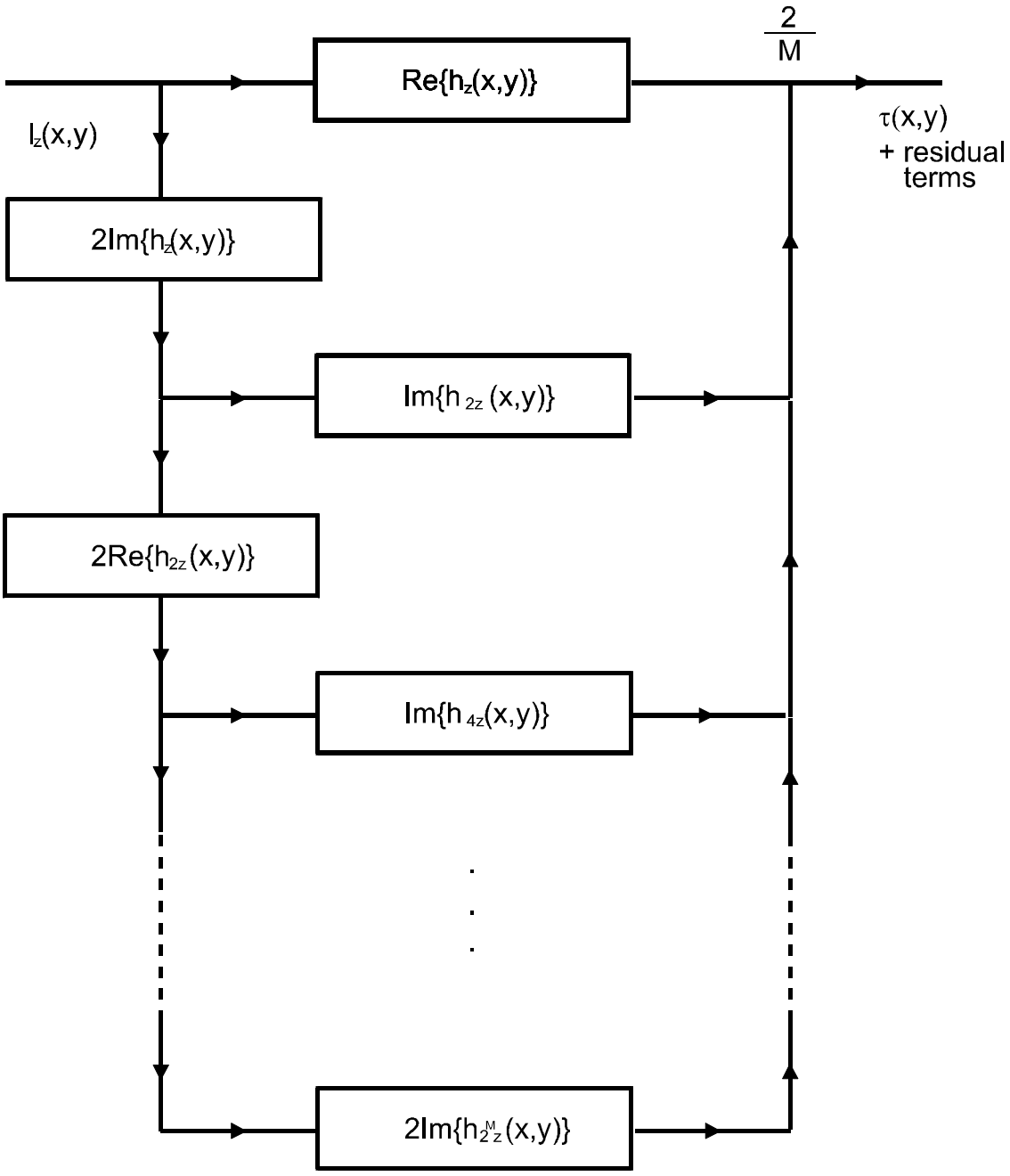

Fig. 4.1 Truncated twin image elimination filter

4.2 Digital implementation of the twin image elimination algorithm

The twin image elimination filter can be effectively implemented in the Fourier domain. The Fourier transform of the functions shown in figure 4.1 are

$$\mathcal{F}\{Re\{h_{2^n z}\}\} = cos\frac{\lambda 2^n z}{4\pi}\left(u^2 + v^2\right), \text{ and} \qquad (4.2-1)$$

$$\mathcal{F}\{Im\{h_{2^n z}\}\} = -sin\frac{\lambda 2^n z}{4\pi}\left(u^2 + v^2\right). \qquad (4.2-2)$$

The filter shown in figure 4.1 can be represented in the Fourier domain as shown in figure 4.2. The structure given in figure 4.2 for the computation of the filter is more efficient than the direct implementation of equation$(4.1-8)$, because convolutions become multiplications in the Fourier domain. The digital decoding of in-line holograms with suppression of the twin image, is achieved by the digital implementation of the filter shown in figure 4.2.

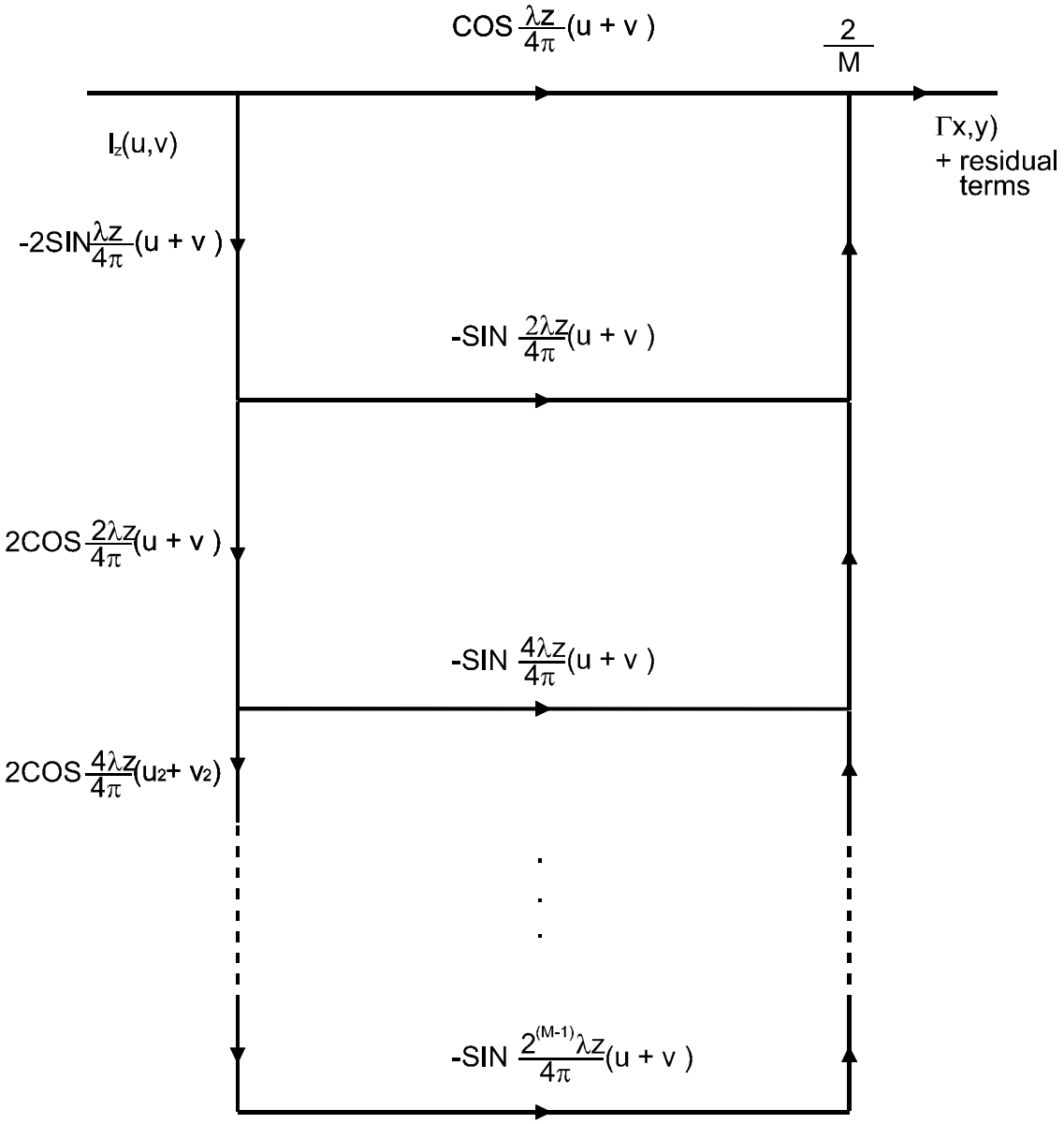

Fig. 4.2 Truncated twin image elimination filter in the Fourier transformation domain

4.3 Adjusted digital filter to overcome Nyquist limitation

We showed that the filtered image converges to the original image without twin image as the number of recursive loops goes to infinity in continuous real space. But in a digital realization of this filter, there is a lack of compactness in discrete space. Thus we must consider the band width that is limited by the sampling rate. From the sampling theorem, the sampled signal is band limited.

$$(U,\ V) = \left(\frac{1}{\Delta x}, \frac{1}{\Delta y}\right) \qquad (4.3-1)$$

$$(X, Y) = \left(\frac{1}{\Delta u}, \frac{1}{\Delta v}\right) \qquad (4.3-2)$$

where $(U,\ \ V), (\Delta x, \Delta y)$ are the band limits and the sampling interval in the space domain respectively, and $(\ X, Y), (\Delta u, \Delta v)$ are the space limit and sampling interval in the frequency domain. Let us consider the components of the filter in the frequency domain. Each component in the frequency domain for the nth loop are $cos\frac{\lambda 2^n z}{4\pi}(u^2+v^2)$, $sin\frac{\lambda 2^n z}{4\pi}(u^2+v^2)$. The local spatial frequency of components in the frequency domain for the nth loop at $(u, v) = (u', v')$ is $\left(\frac{\lambda 2^n z}{2\pi}u', \frac{\lambda 2^n z}{2\pi}v'\right)$. Unfortunately, the spatial frequency of the filter increases as the loop continues but the spatial frequency in discrete space is limited as shown in equation $(4.3-2)$ by the Nyquist sampling theorem. In discrete space, the spatial frequency of the function must be smaller than the spatial frequency limit. If the frequency of the function is larger than the cutoff frequency, there is an aliasing noise due to under sampling. Therefore, the spatial frequency of each component must be located within the spatial band width:

$$\left(\frac{\lambda 2^n z}{2\pi}u', \frac{\lambda 2^n z}{2\pi}v'\right) \leq (X, Y) \qquad (4.3-3)$$

This is a very severe restrictions for the truncated filter, because the spatial frequency of each component increases geometrically as n increases, as seen in equation $(4.3-3)$. To overcome this severe restriction, we propose the an adjusted digital filter. Since the spatial frequency of the filter components depends on both the number of loops and the frequency, as seen in equation $(4.3-3)$, we can express the condition that (u', v') must satisfy after a fixed number of loops$(n = M)$:

$$\left(\frac{\lambda 2^M z}{2\pi}u', \frac{\lambda 2^M z}{2\pi}v'\right) \leq (X, Y) \text{ , or} \qquad (4.3-4)$$

$$(u', v') \leq \left(\frac{4\pi X}{2^{M-1}\lambda z}, \frac{4\pi Y}{2^{M-1}\lambda z}\right) \qquad (4.3-5)$$

If (u', v') is larger than $\left(\frac{4\pi X}{2^{M-1}\lambda z}, \frac{4\pi Y}{2^{M-1}\lambda z}\right)$, aliasing noise will result. Thus we cut the part of filter component which is larger than $\left(\frac{4\pi X}{2^{M-1}\lambda z}, \frac{4\pi Y}{2^{M-1}\lambda z}\right)$, and set that part equal to zero. This component of the filter is given by

$$cos\frac{\lambda 2^n z}{4\pi}\left(u^2+v^2\right)rect\left(\frac{u}{u_m^n}, \frac{u}{v_m^n}\right), \qquad (4.3-6)$$

$$sin\frac{\lambda 2^n z}{4\pi}\left(u^2+v^2\right)rect\left(\frac{u}{u_m^n}, \frac{u}{v_m^n}\right)$$

where$(u_M^n, v_M^n)$is the maximum frequency in discrete space that satisfies inequality $(4.3-5)$ in the nth loop.

Through this process, we can apply more loops without introducing aliasing noise and consequently obtain a better elimination of the twin image in reconstruction. This adjusted twin image elimination digital filter is shown in figure 4.3.

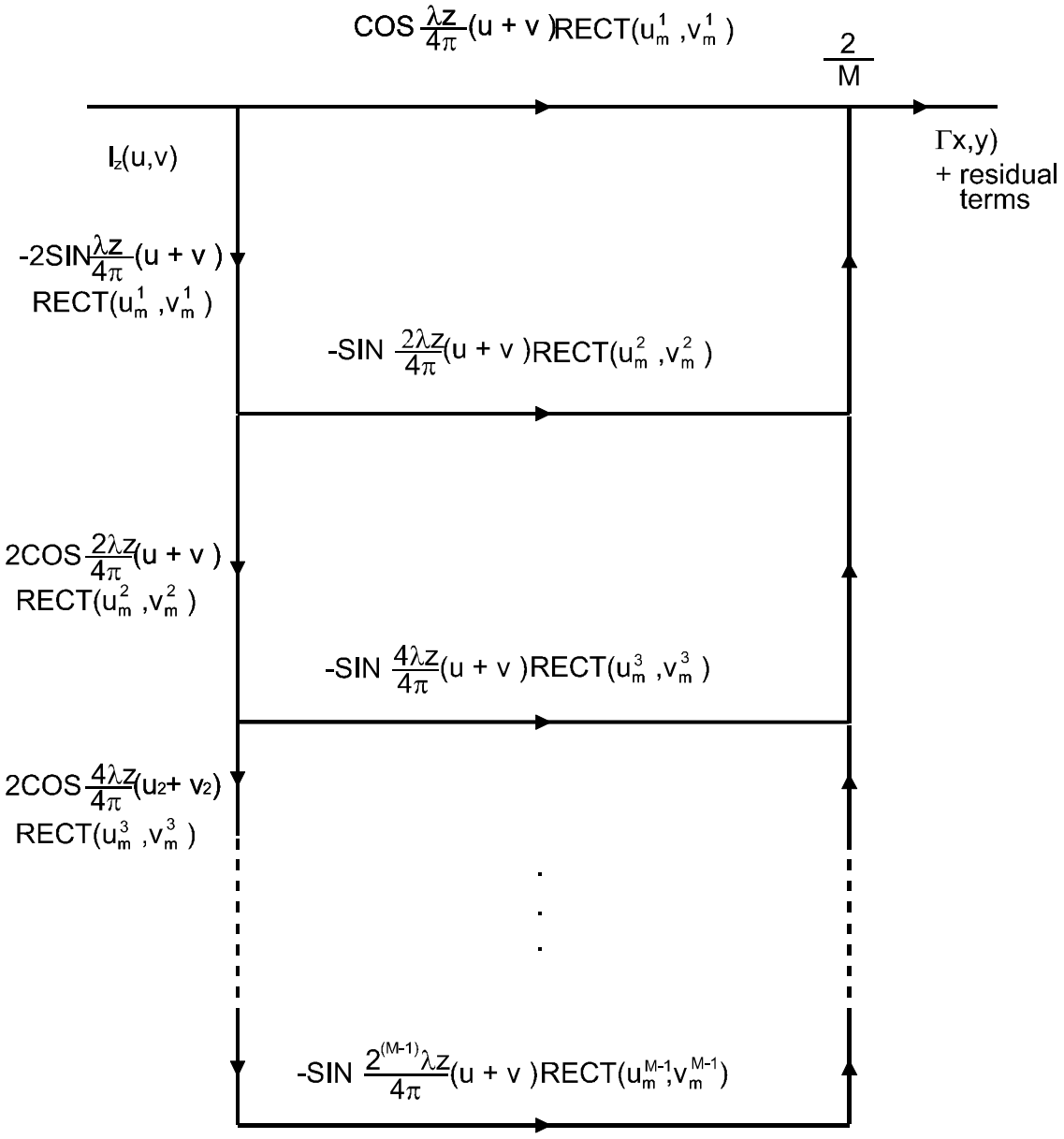

Fig. 4.3 Adjusted truncated twin image elimination filter in the Fourier transformation domain

The comparison between the truncated twin image elimination filter and the adjusted one can be seen in Figures 4.4 to 4.7. Figure 4.4 shows the unfiltered image with the twin image noise. Figure 4.5 and 4.6 show the filtered images by truncated elimination filter and by adjusted elimination filter, respectively. For comparison, figures 4.7 shows the reconstruction with completely eliminated twin image noise using the electronic multiplexing method.

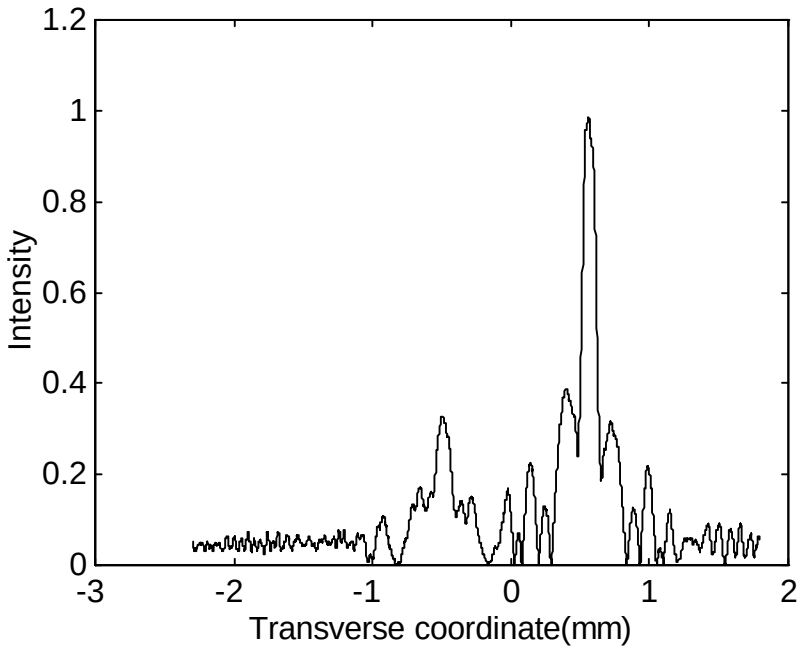

Fig. 4.4 Reconstruction with twin image noise

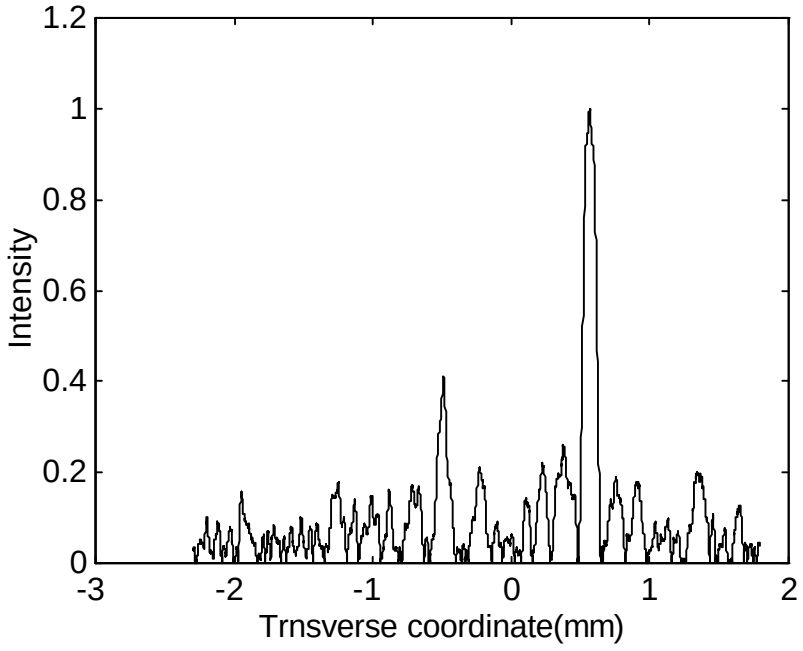

Fig. 4.5 Filtered image with truncated twin image elimination filter

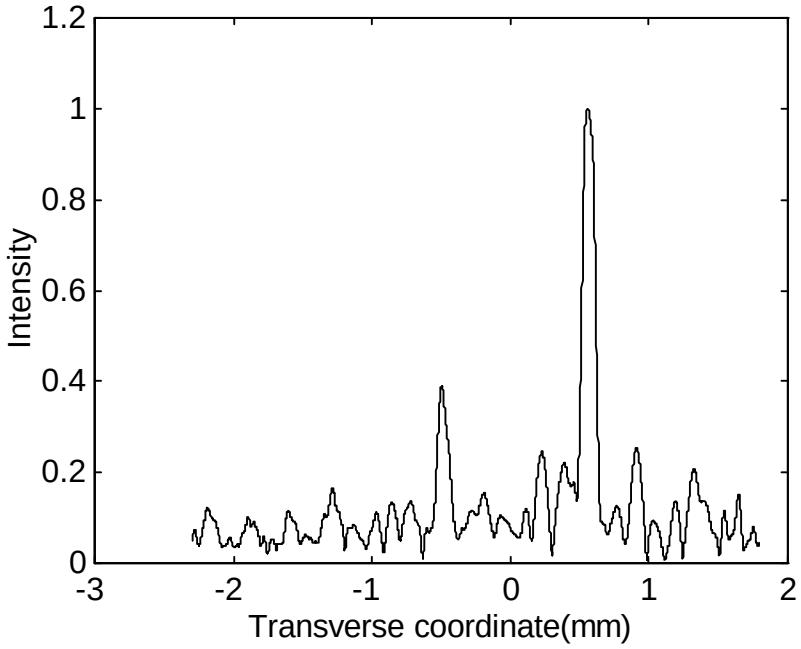

Fig. 4.6 Filtered image with adjusted twin image elimination filter

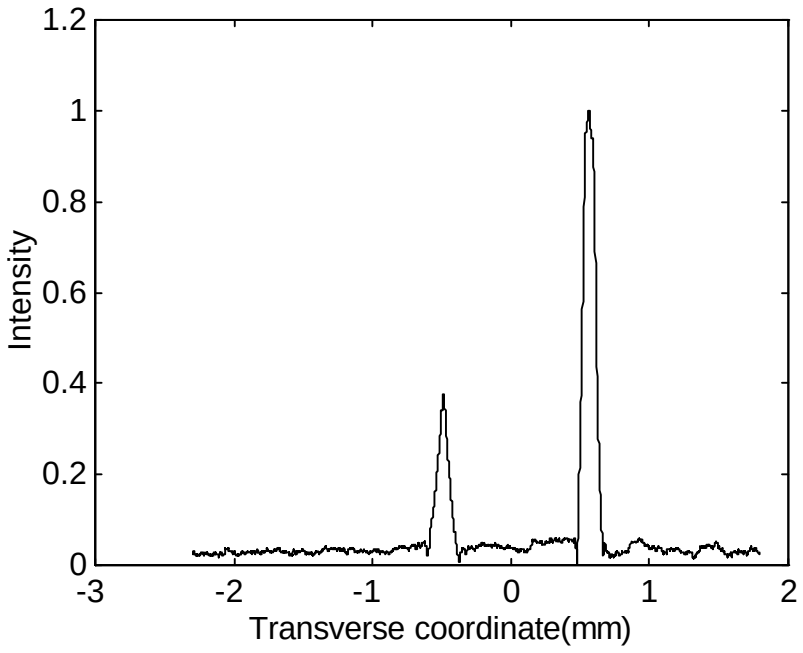

Fig. 4.7 Reconstructed image using multiplexing method

Chapter 5 Conclusion

In this thesis, I have accomplished 3 things: 1, I have shown that the 3-D location of fluorescent objects in a turbid medium can be achieved through a 2-D optical scanning, as a form of holography. This means that we can extract 3-D information about fluorescent objects in a turbid medium with a single 2-D scan. 2, I have analyzed two diffused wave rejecting processes provided by the heterodyne method, the first based on the temporal stretching of pulse, characteristic of diffused photons and the other based on the random varying phase characteristic of the diffuse photons distorting the Fresnel zone pattern. 3, I have applied and tested an electronic multiplexing to eliminate the twin image noise in optical scanning holography, and we proposed and tested an adjusted digital filtering method to overcome the Nyquist limitation of the iterative algorithm used to eliminate the twin image.

To our knowledge, concerning the 3-D imaging of objects in turbid media, this is the first time a 3-D image of fluorescent objects in turbid media has been achieved using a holographic method. The presented system for 3-D imaging in this thesis has advantages for the imaging of fluorescent objects in turbid media. The advantages include the rejection of the diffuse photons by the use of the temporal heterodyne and the holographic selection process due to the fact that the part of the Fresnel zone pattern that is distorted by random scattering does not much contribute to the formation of the hologram of the object, together with the fact that, for recording of 3-D object, a single 2-D scan is needed. These advantages make the optical scanning holographic technique suitable for 3-D imaging of fluorescent objects in turbid media. This can lead to applications in biomedical imaging. A variety of research has recently been conducted to study the fluorescence in human tissues. It has been shown that one can enhance the contrast between diseased and normal tissue by the use of fluorescent properties, rather than absorption or elastic scattering, and one can obtain diagnostic information more easily. For

example, one can use exogenous dyes, which are known to exhibit fluorescence with a high quantum yield as a source of contrast. A number of studies have demonstrated some photosensitizing agents that are selectively observed by tissues, such as hematoporphyrin derivative in neoplastic lesions [17]. These kinds of photo-sensitizing agents could provide fluorescent makers with high quantum yield, which could serve to locate lesions embedded in various organs.

References

1. B. Chance, R. R. , Alfano and A. Katzir, eds, "Optical Tomography, Photon Migration, and Spectroscopy of Tissue and Model Media: Theory, Human Studies, and Instrumentation" SPIE Vol. 2389, Bellingham, Washington, (1995).

2. R. R. Alfano and J. G. Fujimoto, eds,"Advances in Optical Imaging and Photon Migration" Opt. Soc. Am., TOPS Vol. 2, Washington DC, (1996).

3. E. Sevick-Muraca and D. Benaron, eds, "Biomedical Optical Spectroscopy and Diagnostics" Opt. Soc. Am., TOPS Vol.3, Washington DC, (1996).

4. L. Wang and P. P. Ho, eds, "Ballistic 2-D Imaging Through Scattering Walls Using an Ultrafast Optical Kerr Gate" Science, Vol. 253, pp. 769-771 (1991).

5. See the section "Physics of Fluorescence Generation in Tissues" in Ref. 3.

6. B. B. Das, F. Liu and R.R. Alfano, Rep. Prog. Phys. Vol. 60, pp. 227- (1997)

7. M. A. O'Leary, D. A. Boas, B. Chance and A. G. Yodh, J. Luminescence 60, 61 ,pp. 281- (1994).

8. T. C. Poon, "Scanning Holography and two-dimensional image processing by acousto-optic two-pupil synthesis" J. Opt. Soc. Am. A Vol. 4., pp. 521-527 (1985).

9. Bradley D. Duncan and T. C. Poon, "Gaussian beam analysis of optical scanning holography" J. Opt. Soc. Am. A, Vol. 9, pp. 229-236 (1992).

10. K. B. Doh et al., "Twin image elimination in optical scanning holography," Optics & Laser Technology, Vol. 28, No. 2, pp.135-141 (1996). , Vol. 28, No. 2, pp.135-141 (1996).

11. B. W. Schilling, and T. C. Poon, " ", Optics letter., in press

12. Elizabeth M. Slayter, Optical Methods in Biology, Wiley-Interscience, New York, 1970.

13. Akira Ishimaru, Wave Propagation and Scattering in Random Media, Academic Prress, New York, 1978.

14. K. B. Doh, T. C. Poon and Guy Indebetouw, "Twin-image noise in optical scanning holography", Opt. Eng. Vol.35, No. 6, pp. 1550-1555 (1996).

15. L. Onural and Peter D. Scott, " Digital decoding of in-line holograms", Opt. Eng. Vol. 26, No. 11, pp. 1124-1132 (1987).

16. K.M. Yoo and R.R. Alfano, "Time resolved coherent and incoherents of forward light scattering in random media ", Optics letters Vol. 15, NO. 6 March 15, pp. 320-322 (1990).

17. J. F. Evensen, S. Sommer, J. Moan, and T. Christensen, "Tumor-localizing and photosensitizing properties of the main components of hematoporphyrin derivative," Cancer Res. 44 482-486 (1986).

Vita

Taegeun Kim was born in Seoul, Korea, on November 23, 1972. He received the B.S degree in Electroincs Engineering form Kyung Hee University, Seoul, Korea in 1996. He then joined the Electrical and Computer Engineering Department at Virginia Polytechnic Institute and State University as a graduate student. He joined optical image processing Laboratory in 1996, where he has been a research assistant. His research interests include holography, optical information processing, digital image processing, optical communication and fiber optics.